A microelectromechanical system for thermomechanical testing of nanostructures

Tzu-Hsuan Chang and Yong Zhu

Citation: Applied Physics Letters **103**, 263114 (2013); doi: 10.1063/1.4858962
View online: http://dx.doi.org/10.1063/1.4858962
View Table of Contents: http://scitation.aip.org/content/aip/journal/apl/103/26?ver=pdfcov
Published by the AIP Publishing

A microelectromechanical system for thermomechanical testing of nanostructures

Tzu-Hsuan Chang and Yong Zhu[a)]
Department of Mechanical and Aerospace Engineering, North Carolina State University, Raleigh, North Carolina 27695, USA

(Received 13 October 2013; accepted 11 December 2013; published online 30 December 2013)

We report an integrated microelectromechanical system (MEMS) with an on-chip heater for *in-situ* mechanical testing of nanostructures from room to elevated temperatures. Multiphysics simulation is used to predict the temperature distribution in air and vacuum conditions. The temperature simulation in air agrees well with the measurement based on Raman spectroscopy. Mechanical testing of single crystalline silicon nanowires is carried out to investigate the brittle-to-ductile transition, demonstrating the efficacy of the MEMS stage. The stage reported here could be applied to investigate the temperature effect on mechanical properties at the nanoscale. © *2013 AIP Publishing LLC*. [http://dx.doi.org/10.1063/1.4858962]

One-dimensional (1D) nanostructures, such as crystalline nanowires, are critical building blocks of nanotechnology applications.[1,2] In addition, they provide an ideal testbed to probe fundamental mechanical behavior at the nanoscale.[3,4] At room temperature, crystalline nanowires exhibit size dependent mechanical properties (e.g., Young's modulus and fracture strength)[5–10] and deformation mechanisms (e.g., dislocation nucleation from free surfaces).[10–12] How about their mechanical properties and deformation mechanisms at elevated temperatures? One question of interest is brittle-to-ductile transition (BDT). Preliminary evidence showed that the BDT temperature of single crystalline silicon (SCS) reduces with sample size.[13–16] It is however unclear if SCS nanowires exhibit ductility at room temperature. Han *et al*. observed ductile deformation of SCS nanowires with diameter <60 nm at room temperature during *in-situ* tensile testing in a transmission electron microscope (TEM).[14] However, Zhu *et al*. reported no ductility at room temperature, even for SCS nanowires of 16 nm in diameter by quantitative *in-situ* scanning electron microscopy (SEM) tensile testing.[7] The authors argued that electron beam irradiation in TEM could lead to the observed plastic deformation in SCS nanowires. Therefore, *in-situ* nanomechanical testing at varying temperatures is in timely need to further elucidate the nanoscale BDT and other thermally-activated deformation mechanisms at the nanoscale.

In-situ mechanical testing at high temperatures is challenging at small scale. Zupan *et al*. performed tensile testing of millimeter scale samples using resistive (Joule) heating of the samples.[17] Sharpe *et al*. measured the fracture strength of SiC samples (a few hundred micrometers in width) in a furnace.[18] Nakao *et al*. studied plasticity in microscale SCS under bending on top of a hot plate.[16] Haque and Saif measured thermomechanical properties of nanoscale Al films also on top of a hot plate.[19] All the above devices were not compatible with *in-situ* SEM or TEM. Recently, Kang and Saif developed a microfabricated structure with resistive heating that can be placed *in-situ* inside SEM.[20] Yet, the system is quite complicated and the smallest sample was 720 nm in width and 6.5 μm in depth. Although resistive heating of the samples is relatively easy to implement, it was found to cause nonuniform temperature distribution and as a result reduction in yield and ultimate tensile strengths.[21]

In this paper, we report an integrated microelectromechanical system (MEMS) with an on-chip heater for *in-situ* mechanical testing of nanostructures from room to elevated temperatures. Figure 1 shows an overview of the integrated MEMS testing stage, consisting of three parts—an electrostatic actuator, a capacitive load sensor, and a heater based on Joule heating. Fully 3D multiphysics (coupled electrical-thermal-mechanical) simulation was used to predict the temperature distribution in both air and vacuum conditions. The temperature simulation in air agreed well with the measurement based on Raman spectroscopy. The simulation in vacuum was used to predict the temperature distribution for the *in-situ* electron microscopy testing of nanostructures. Mechanical testing of SCS nanowires in SEM was carried out to investigate the BDT, demonstrating the efficacy of the integrated MEMS stage.

The integrated testing stages were fabricated at MEMSCAP (Durham, NC) using the Silicon-on-Insulator Multi-User MEMS Processes (SOI-MUMPs). The microfabrication process is simple and does not add any extra step compared to that for fabricating the pure mechanical testing stage. The stage is made of one layer of SCS with thickness of 10 μm. As shown in Figure 1, the actuator is a comb drive based on electrostatic force, and the heater is based on Joule heating of the SCS structure itself (i.e., no additional metal layer). To achieve independent control of the actuation and heating, the comb drive actuator is used in our design instead of the widely used thermal actuator.[22,23] Under actuation voltage V, the comb drive generates electrostatic force F

$$F = N\frac{\varepsilon t V^2}{d}, \tag{1}$$

where N is the number of finger pairs, ε is the permittivity of vacuum or air depending on the operating environment, t is the comb thickness, and d is the spacing between neighboring

[a)]E-mail: yong_zhu@ncsu.edu

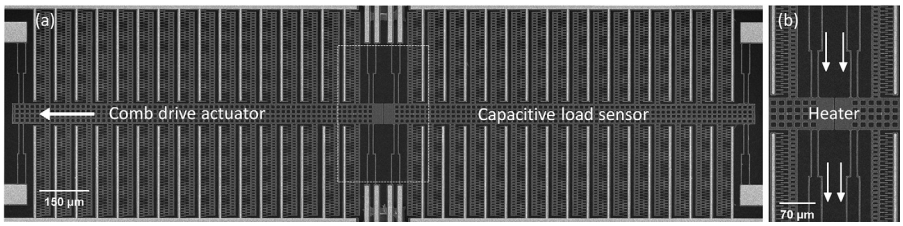

FIG. 1. (a) SEM image of the entire MEMS device that consists of three parts: Comb drive actuator, capacitive load sensor, and heater. (b) Magnified view of the heater as boxed in (a). The arrows indicate the current direction.

combs. A critical part of the integrated stage is the on-chip heater. To achieve identical temperature at both ends of the specimen, the entire stage is symmetric with respect to the specimen. Notably, the sensor has the identical structure as the actuator. For actuation, a voltage is applied between the movable and fixed combs; for sensing, the capacitance can be measured between the movable and fixed combs. When the heater is turned on, the temperature in the shuttle arises and as a result the shuttle elongates due to thermal expansion. In this case, the specimen would be compressed. Since the shuttle is very long compared to the specimen, this compression could be serious. Indeed, in our initial design, a serpentine-like heater was employed (Figure S1); serpentine structure is commonly used in MEMS to reduce its stiffness. As an example, to achieve 326 °C (599 K) temperature (at the heating voltage of ~7.4 V), the gap between the two shuttles reduces 1.06 μm, equivalent to 53% compressive strain imposed on the specimen (the specimen length is equal to the initial gap, 2 μm). New designs to reduce such an undesired thermal displacement must be sought, although it appears not possible to completely eliminate it using the simple microfabrication process in the present study. In general, shielding the thermal displacement from the specimen is challenging at the micro/nano-scale.

Here, we present one design that effectively reduces the thermal displacement to 180 nm over the entire temperature range from room temperature to 599 K. The design is based on the Z-shaped thermal actuator,[22] which provides an additional thermal displacement to counterbalance that due to the shuttle expansion. Note that the Z-shaped beam over the V-shaped beam[23] is selected due to the much lower stiffness (for the comparable dimensions) of the former; low stiffness of the heater is preferred as it takes less load imposed by the comb drive actuator. The key parameter of the Z-shaped design is the length of the central beam, which is easy to adjust. With increasing central beam (>2 μm), the thermal displacement decreases.[22]

Nonlinear multiphysics finite element analysis (FEA) was carried out using ANSYS 13.0 to predict temperature distribution and thermal displacement of the proposed stage both in vacuum and in air.[24] For the vacuum condition, the only heat dissipation mechanism is the heat conduction through the device itself to the anchors (substrate). For the air condition, additional heat dissipation mechanism is thermal conduction through the air to the fixed combs (connected to the substrate). Thermal convection and thermal radiation were found to be negligible in our case. The simulation is a coupled-field analysis involving electric, thermal, and mechanical fields. The electric boundary conditions are the positive and negative voltages at both ends of the heater. The thermal boundary conditions are zero temperature change at the substrate. The mechanical boundary conditions are fixed displacements at the anchors. Element type SOLID 98 was used for the stage (made of SCS) and SOLID 70 was used for the air. The material parameter that used in the simulation are listed in Table I.

Figure 2(a) shows the temperature distribution of the testing stage in vacuum; the heating voltage (across the

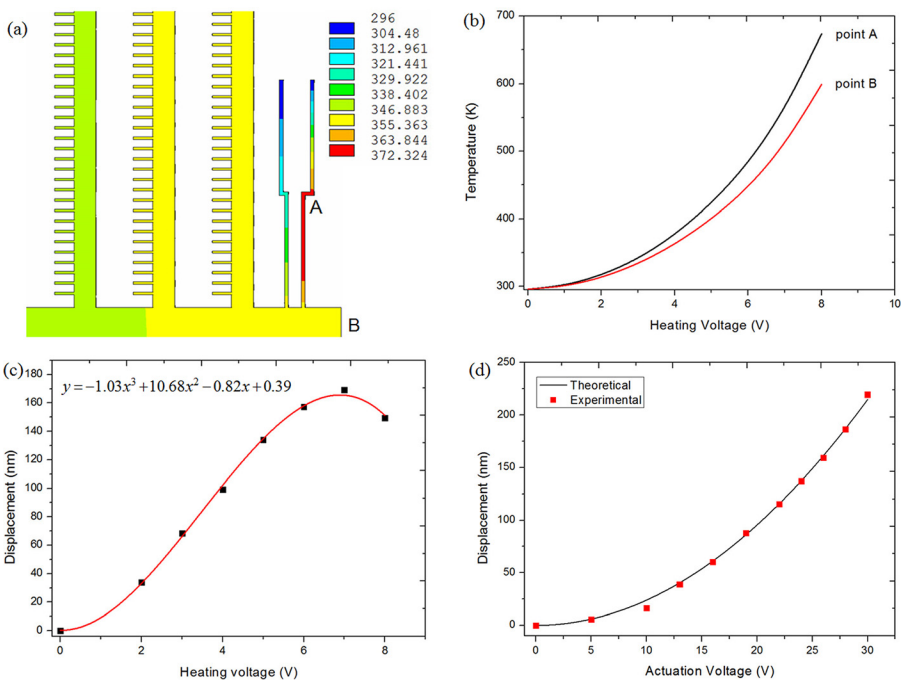

FIG. 2. (a) Simulated temperature distribution under 4 V heating voltage in vacuum, (b) simulated temperature profile at points A and B as functions of heating voltage, (c) measured thermal displacement as a function of heating voltage, (d) displacement of comb drive actuator as a function of actuation voltage at room temperature (theoretical calculation according to Eq. (1)).

heater) is 4 V. Due to symmetry, only a quarter of the stage is shown. The highest temperature does not occur at the center of the heater. This is because of the presence of the support beams on the other side of the comb drive, which provides an additional route for heat dissipation. Figure 2(b) shows the temperatures of two points, A (where the highest temperature is) and B (center of the shuttle, where the specimen is mounted), as functions of the heating voltage. For SCS, plastic deformation for beams of 4 μm width under bending could be as low as ~680 K.[16] In the present work, the heating voltage was always kept below 8 V with the maximum temperature of 599 K at point B (and 650 K at point A). According to our calibration experiment, no permanent deformation or damage to heating beams was observed in this temperature range. Figure 2(c) shows the undesired thermal displacement as a function of the heating voltage. The maximum displacement corresponds to 9% compressive strain in the nanowires. This is the best scenario we have been able to obtain over the entire temperature range from room temperature to 599 K. By contrast, this thermal displacement in a conventional serpentine-type heater is shown in Figure S1,[27] which is about 6 times of that in our present design.

Still the thermal displacement is undesired and should be compensated. Figure 2(d) plots the measured displacement of the comb drive actuator as a function of the actuation voltage, which agrees very well with the theoretical predication, via Eq. (1). The thermal displacement versus the heating voltage can be fitted with a polynomial equation, see Figure 2(c). So by comparing the fitting equation and Eq. (1), it is possible to compensate the undesired thermal displacement with the comb drive motion following:

$$V_A = -0.02V_H^3 - 0.23V_H^2 + 6.47V_H + 0.56, \qquad (2)$$

where V_H is the heating voltage of the heater and V_A is the actuation voltage of the comb drive. As an example, to achieve 599 K temperature in the specimen, 8 V heating voltage is required. Thus, the comb drive should be actuated at 25 V simultaneously to eliminate the undesired thermal displacement.

Figure 3(a) shows the temperature distribution of the testing stage in air for the heating voltage of 4 V, while Figure 3(b) shows the temperatures of two points A and B as functions of the heating voltage. The air in the Figure 3(a) are removed intentionally in order to show a clear relationship between free comb and fixed comb. For the original contour plot of simulation result, please see supporting information.[27] The temperature was measured using a HORIBA LabRAM HR Raman microscope in air (laser wavelength 633 nm). The laser power was kept below 0.003 mW to avoid laser-induced local heating. Each measurement took approximately 60 s. The Stokes shift was recorded and analyzed in our experiments. The Raman spectra were fit to a Voight lineshape function to determine the Stokes peak location. It is seen that with increasing actuation voltage, the Stokes peak blue-shifted. Following the calibration experiment reported previously,[24] the change in the peak position can be converted to the temperature rise in the heater, viz.

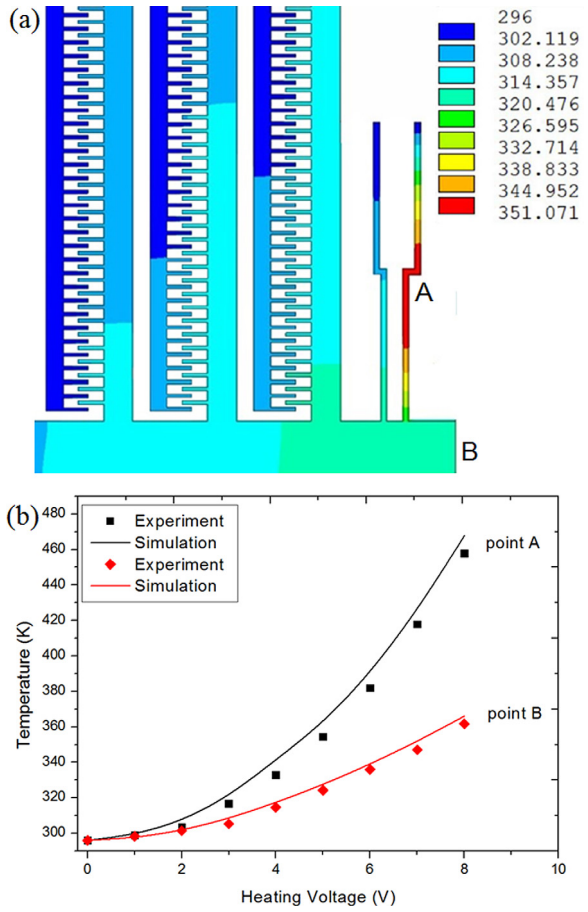

FIG. 3. (a) Simulated temperature distribution under 4 V heating voltage in air, (b) temperatures profile at points A and B as functions of heating voltage in air.

$$\Delta T = \frac{\Omega - \Omega_0}{-0.0242\,\mathrm{cm}^{-1}}\frac{K}{}, \qquad (3)$$

where Ω_0 and Ω are the measured peak positions at the laboratory temperature of 296 K and at the operating temperature, respectively. Simulated and measured temperatures at points A and B agreed very well (Figure 3(b)), which indicates the accuracy of the FEA simulations and verifies the predicting power of the simulation performed in vacuum (for *in-situ* SEM testing). The verification is important, as we are currently not capable of measuring temperature in SEM with the required spatial resolution on the order of μm. In addition, the temperatures on point B and the middle of the nanowire were measured before the mechanical testing, which confirmed that the temperatures are the same. (Details on the Raman measurement and multiphysics simulation are provided in supplementary material)[27]

To demonstrate the efficacy of the integrated thermomechanical testing stage, it was used to test SCS nanowires *in-situ* inside a SEM (FEI Quanta 3D FEG) to probe their BDT. The SCS nanowires were manipulated and positioned onto the MEMS stage following the pick-place method.[25] Figures 4(a) and 4(b) show a SCS nanowire (with diameter of 60 nm) clamped on the testing stage before and after the thermomechanical testing, respectively. Figure 4(c) shows the loading-unloading behavior of the SCS nanowire at different temperatures. Tensile testing was initially conducted at room

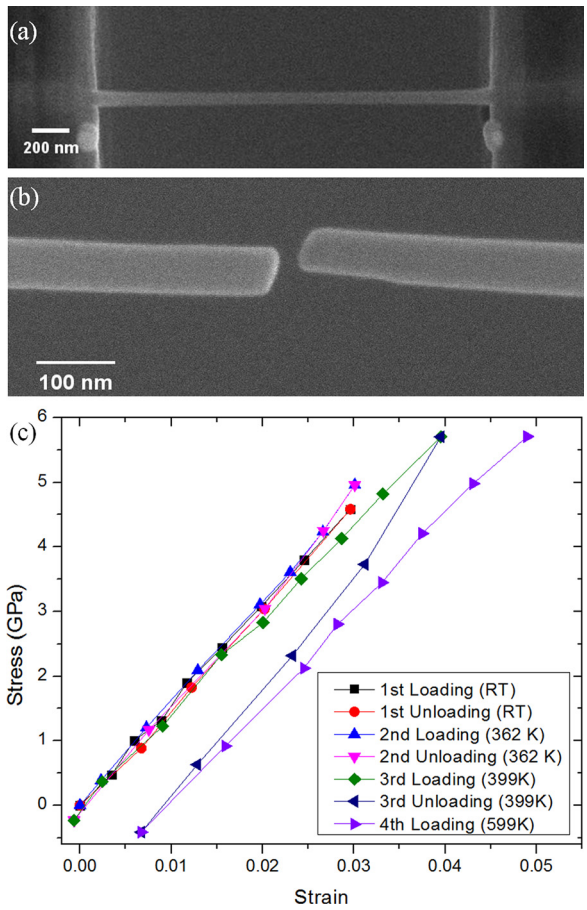

FIG. 4. SEM images showing a SCS nanowire with diameter of 60 nm on the MEMS stage (a) before and (b) after the thermomechanical testing, (c) stress-strain curve of the SCS nanowire under different temperatures (1st, 2nd, 3rd, and 4th loading corresponding to room temperature, 362 K, 399 K, and 599 K, respectively).

temperature, and then done at gradually increasing temperatures. It can be seen that the first and second loading and unloading curves, which represent temperature at room temperature and 362 K, followed identical linear paths. No plastic deformation was observed when the nanowire was fully unloaded. The Young's modulus at room temperature was measured to be 164 GPa. However, as temperature was increased to 399 K (the third loading and unloading curve), yielding was observed with 0.5% plastic strain after the nanowire was totally unloaded. This stress-strain behavior suggested that the BDT temperature of the SCS nanowire (with diameter of 60 nm) lies between 362 K and 399 K, which is much lower than those of bulk SCS (>900 K) and micro-scale SCS (>600 K). The nanowire was broken at 599 K during the fourth loading curve with a failure strain of ~4.9%, which is substantially higher than the fracture strain of SCS nanowire of the same diameter at room temperature (~2.8%).[7] The fracture surfaces, as shown in Figure 4(b), tilt with respect to the nanowire loading axis, indicating shear failure, which is in contrast to the cleavage fracture observed at room temperature.[7] The observed fracture surface agrees very well with that predicted by molecular dynamics simulations for SCS nanowires at high temperature.[26] The above fractography and stress-strain behavior unambiguously reveal the presence of plasticity in SCS nanowires at elevated temperatures. Our finding is the first quantitative assessment of BDT in SCS nanowires under tensile loading.

TABLE I. Material parameters used in the simulations.[24]

Parameter	Symbol	Value	Unit
Young's modulus	E	160	GPa
Poisson ratio	v	0.28	…
Thermal conductivity of Si	$K_{Si}(T)$	$210658 \times T^{-1.2747}$	W/(mK)
Thermal conductivity of air	K_{air}	0.026	W/(mK)
Free convection coefficient of air	C_{air}	20	W/(m^{2}K)
Thermal expansion coefficient	$\alpha(T)$	$-4 \times 10^{-12}T^2 + 8 \times 10^{-9} T + 4 \times 10^{-7}$	K^{-1}
Resistivity	$\rho(T)$	$5.1 \times 10^{-5} [1 + 3 \times 10^{-3}(T - 273)]$	Ωm

In summary, we report an integrated MEMS stage for thermomechanical testing of 1D nanostructures. The temperature predicted by 3D multiphysics simulation in air agreed very well with that measured by Raman spectroscopy. Then the simulation was used to predict the temperature distribution in vacuum for the *in-situ* electron microscopy testing of nanostructures. Mechanical testing of SCS nanowires in SEM was carried out to investigate the BDT, demonstrating the efficacy of the integrated MEMS stage. A SCS nanowire of 60 nm in diameter exhibited linear elastic behavior at room temperature but plasticity and ductile failure above 399 K. Temperature effects on mechanical properties of nanostructures are interesting, but so far have been much less studied at least experimentally. The MEMS testing stage reported here could greatly enhance the instrumentation capabilities for probing the thermomechanical properties at the nanoscale.

This project was supported by the National Science Foundation under Award Nos. CMMI-1030637 and 1301193. The SEM experiments were performed in the Analytical Instrumentation Facility at North Carolina State University.

[1]Y. Xia, P. Yang, Y. Sun, Y. Wu, B. Mayers, B. Gates, Y. Yin, F. Kim, and H. Yan, Adv. Mater. **15**, 353 (2003).
[2]F. Xu, W. Lu, and Y. Zhu, ACS Nano **5**, 672 (2011).
[3]H. S. Park, W. Cai, H. D. Espinosa, and H. Huang, MRS Bull. **34**, 178 (2009).
[4]T. Zhu and J. Li, Prog. Mater. Sci. **55**, 710 (2010).
[5]C. Q. Chen, Y. Shi, Y. S. Zhang, J. Zhu, and Y. J. Yan, Phys. Rev. Lett. **96**, 75505 (2006).
[6]R. Agrawal, B. Peng, E. Gdoutos, and H. D. Espinosa, Nano Lett. **8**, 3668 (2008).
[7]Y. Zhu, F. Xu, Q. Q. Qin, W. Y. Fung, and W. Lu, Nano Lett. **9**, 3934 (2009).
[8]F. Xu, Q. Q. Qin, A. Mishra, Y. Gu, and Y. Zhu, Nano Res. **3**, 271 (2010).
[9]L. G. Zhou and H. C. Huang, Appl. Phys. Lett. **84**, 1940 (2004).
[10]Y. Zhu, Q. Q. Qin, F. Xu, F. R. Fan, Y. Ding, T. Zhang, B. J. Wiley, and Z. L. Wang, Phys. Rev. B **85**, 45443 (2012).
[11]T. Zhu, J. Li, A. Samanta, A. Leach, and K. Gall, Phys. Rev. Lett. **100**, 25502 (2008).
[12]H. S. Park, K. Gall, and J. A. Zimmerman, J. Mech. Phys. Solids **54**, 1862 (2006).
[13]W. Kang and M. T. A. Saif, Adv. Funct. Mater. **23**, 713 (2013).
[14]X. Han, K. Zheng, Y. F. Zhang, X. Zhang, Z. Zhang, and Z. L. Wang, Adv. Mater. **19**, 2112 (2007).

[15]F. Ostlund, K. Rzepiejewska-Malyska, K. Leifer, L. M. Hale, Y. Y. Tang, R. Ballarini, W. W. Gerberich, and J. Michler, Adv. Funct. Mater. **19**, 2439 (2009).
[16]S. Nakao, T. Ando, M. Shikida, and K. Satol, J. Micromech. Microeng. **16**, 715 (2006).
[17]M. Zupan, M. J. Hayden, C. J. Boehlert, and K. J. Hemker, Exp. Mech. **41**, 242 (2001).
[18]W. N. Sharpe, O. Jadaan, G. M. Beheim, G. D. Quinn, and N. N. Nemeth, J. Microelectromech. Syst. **14**, 903 (2005).
[19]M. A. Haque and M. T. A. Saif, Thin Solid Films **484**, 364 (2005).
[20]W. Kang and M. T. A. Saif, J. Micromech. Microeng. **21**, 105017 (2011).
[21]N. J. Karanjgaokar, C.-S. Oh, and I. Chasiotis, Exp. Mech. **51**, 609 (2011).
[22]C. H. Guan and Y. Zhu, J. Micromech. Microeng. **20**, 85014 (2010).
[23]Y. Zhu, A. Corigliano, and H. D. Espinosa, J. Micromech. Microeng. **16**, 242 (2006).
[24]Q. Qin and Y. Zhu, Appl. Phys. Lett. **102**, 013101 (2013).
[25]Y. Zhu and H. D. Espinosa, Proc. Natl. Acad. Sci. U.S.A. **102**, 14503 (2005).
[26]K. W. Kang and W. Cai, Int. J. Plast. **26**, 1387 (2010).
[27]See supplementary material at http://dx.doi.org/10.1063/1.4858962 for the design with a serpentine-type heater, the simulated temperature contour plot in air, and details on the Raman measurement and multiphysics simulation.